Superconductivity in Expanded fcc C_{60}^{3-} Fullerides

Patrik Dahlke, Mark S. Denning, Paul F. Henry, and Matthew J. Rosseinsky*,†

Contribution from the Inorganic Chemistry Laboratory, Department of Chemistry, University of Oxford, South Parks Road, Oxford OX1 3QR, U.K.

Received August 2, 2000

Abstract: The behavior of A_3C_{60} superconductors at the large inter-fulleride separation where the transition temperatures (T_c) are highest is investigated by the synthesis and structural and electronic characterization of face-centered cubic (fcc) A_3C_{60} compounds with the largest lattice parameters yet found. In this family T_c *decreases* with increasing inter-fulleride separation, despite a continued increase in the density of states at the Fermi level. This contrasts with $T_c(a)$ relationships previously demonstrated for these materials and is consistent with recent suggestions that the interelectron repulsions between carriers in the t_{1u} band are important in determining T_c in a fulleride metal near the Mott−Hubbard transition.

Introduction

The A_3C_{60} alkali metal fullerides[1,2] have the highest superconducting transition temperatures (T_c) apart from the copper oxides. T_c reaches a maximum of 33 K in Cs_2RbC_{60}[3] in the face-centered cubic (fcc) family, while the highest reported value for a fulleride salt is 40 K under 15 kbar hydrostatic pressure for Cs_3C_{60}, which adopts a body-centered packing.[4] A key experimental observation is that T_c increases monotonically with the inter-fulleride separation in the widely studied fcc phases.[5−9] This is consistent with the well-known BCS-McMillan theory in which T_c is controlled by the density of electronic states at the Fermi level, $N(E_f)$, which increases together with the intermolecular separation as a direct consequence of the reduction in the width of the band derived from the t_{1u} frontier orbitals of the C_{60}^{3-} anions.

Testing of this understanding of T_c, and the search for higher superconducting transition temperatures in the fulleride family, requires the synthesis of fcc phases with larger lattice parameters to further decrease the intermolecular overlap between t_{1u} orbitals. In this paper, we demonstrate that the widely accepted BCS-McMillan treatment is incapable of describing the behavior of the fcc A_3C_{60} series at large lattice parameters, by preparing and structurally and electronically characterizing Cs-rich fcc A_3C_{60} phases. In this family, T_c is *lower* than for the smaller *a* Cs_2RbC_{60} and *decreases* with increasing lattice parameter, although the density of states at the Fermi level ($N(E_f)$) increases as expected. Rietveld refinement of synchrotron X-ray data does not indicate significant positional disorder of the octahedral cesium cation, in contrast with the $A_2Na(NH_3)C_{60}$ phases[10] where T_c decreases with increasing *a* despite an increase in $N(E_f)$.[11] This behavior presents a well-defined challenge for theory in the region of the highest fulleride superconducting transition temperatures. The stability of the metallic state at the observed low fulleride densities is of general importance for correlated electron systems and can be attributed to the t_{1u} orbital degeneracy stabilizing itinerant over localized states.

Experimental Section

Synthesis. All manipulations were carried out in a helium-filled drybox (with oxygen/moisture levels low enough to allow a 25-W light bulb to burn for 3 days) and a dual-manifold high-vacuum line. Samples of overall composition $Cs_{3-x}Rb_xC_{60}$ ($0.3 < x < 0.34$) and $Cs_{3-x}K_xC_{60}$ ($0.3 < x < 0.74$) were prepared by reduction of sublimed C_{60} using the metals dissolved in liquid ammonia at −78 °C.[4,12] The metals and C_{60} were added in stoichiometric amounts calculated for 0.06 mmol of product into the two legs of a Pyrex H-cell reaction vessel. The metals and the C_{60} powder were loaded into opposite legs of the cell to prevent mixing before complete solvation of the metals has taken place. Sixty milliliters of predried (over sodium) liquid ammonia was transferred onto the metals. More dilute conditions led to lower yields and larger phase fractions for the *Immm* and *Pm*3*n* Cs_xC_{60} impurity phases. The blue metal ammonia solution was poured onto the C_{60}, and the reaction mixture was shaken to ensure complete mixing. It was found that the method of mixing did not significantly affect the phase purity. Raising the reaction temperature to −48 °C decreased the yield of the fcc phase. About 10 min after the initial mixing, a red color indicating the presence of the soluble C_{60}^{3-} anion appears and no further color change of the solution is observed. After 120 min, the ammonia was removed, finally by evacuating the H-cell overnight at room temperature to a final pressure of below 10^{-4} Torr. The resulting powder was ground in the drybox, heated at 120 °C for 6 h under dynamic vacuum to a base pressure of 1×10^{-5} Torr, and sealed in a Pyrex vessel. The ammonia content of the material was investigated by weight loss and CHN microanalysis at the different stages of the synthesis.

† Current address: Department of Chemistry, University of Liverpool, Robert Robinson Laboratories, Liverpool, L69 7ZD, U.K. E-mail: m.j.rosseinsky@liv.ac.uk.

(1) Rosseinsky, M. J. *Chem. Mater.* **1998**, *10*, 135.
(2) Prassides, K. *Curr. Opin. Solid State Mater. Sci.* **1997**, *2*, 433−439.
(3) Tanigaki, K.; Ebbesen, T. W.; Saito, S.; Mizuki, J.; Tsai, J. S.; Kubo, Y.; Kuroshima, S. *Nature* **1991**, *352*, 222.
(4) Palstra, T. T. M.; Zhou, O.; Iwasa, Y.; Sulewski, P. E.; Fleming, R. M.; Zegarski, B. R. *Solid State Commun.* **1995**, *93*, 327.
(5) Fleming, R. M.; Ramirez, A. P.; Rosseinsky, M. J.; Murphy, D. W.; Haddon, R. C.; Zahurak, S. M.; Makhija, A. V. *Nature* **1991**, *352*, 787−788.
(6) Sparn, G.; Thompson, J. D.; Huang, S.-M.; Kaner, R. B.; Diederich, F.; Whetten, R. L.; Gruner, G.; Holczer, K. *Science* **1991**, *252*, 1829.
(7) Zhou, O.; Vaughan, G. B. M.; Zhu, Q.; Fischer, J. E.; Heiney, P. A.; Coustel, N.; McCauley, J. P.; Smith, A. B. *Science* **1992**, *255*, 833.
(8) Chen, C. C.; Kelty, S. P.; Lieber, C. M. *Science* **1991**, *253*, 886.
(9) Movshovich, R.; Thompson, J. D.; Chen, C. C.; Lieber, C. M. *Phys. Rev. B* **1994**, *49*, 3619.
(10) Iwasa, Y.; Shimoda, H.; Miyamoto, Y.; Mitani, T.; Maniwa, Y.; Zhou, O.; Palstra, T. T. M. *J. Phys. Chem. Solids* **1997**, *58*, 1697.
(11) Maniwa, Y.; Sugiura, D.; Kume, K.; Kikuchi, K.; Suzuki, S.; Achiba, Y.; Hirosawa, I.; Tanigaki, K.; Shimoda, H.; Iwasa, Y. *Phys. Rev. B* **1996**, *54*, R6861.
(12) Ziebarth, R. P.; Buffinger, D. R.; Stenger, V. A.; Recchia, C.; Pennington, C. H. *J. Am. Chem. Soc.* **1993**, *115*, 9267.

10.1021/ja002861d CCC: $19.00
Published on Web 11/23/2000

Table 1. Structural Properties of the Expanded fcc A_3C_{60} Phases with fcc Phase Fractions (Determined by Rietveld Refinement of Powder X-ray Diffraction Data) of over 65% (a)[a] and Superconducting Properties of Expanded fcc A_3C_{60} Phases (b)[c]

(a) Structural Properties

nominal composition	refined composition of fcc phase	fcc phase fraction, %	fractional occupation of Cs on O and T sites[d]		*a*, Å	V/C_{60}, Å^{-3}	annealing time, d^{-1}, at °C	refined impurity phase(s)
			O	T				
$Cs_{2.26}K_{0.74}C_{60}$	**$Cs_{2.07(2)}K_{0.93(2)}C_{60}$**	**92(1)**	**0.93(2)**	**0.57(1)**	**14.570(1)**	**773.2(1)**	**11 at 350**	**Cs_3C_{60}**
$Cs_{2.38}K_{0.62}C_{60}$ a1	**$Cs_{2.03(2)}K_{0.97(2)}C_{60}$**	**72(1)**	**0.71(1)**	**0.66(1)**	**14.581(1)**	**775.0(1)**	**12 at 350**	**Cs_1C_{60}**
$Cs_{2.38}K_{0.62}C_{60}$ a2	$Cs_{2.51(2)}K_{0.49(2)}C_{60}$	100	0.94(1)	0.787(9)	14.646(2)	790.1(2)	23 at 350	
$Cs_{2.38}K_{0.62}C_{60}$ a3	$Cs_{2.51(2)}K_{0.49(2)}C_{60}$	100	0.97(1)	0.77(1)	14.6276(9)	782.5(1)	29 at 350	
$Cs_{2.33}K_{0.67}C_{60}$ b	$Cs_{2.04(3)}K_{0.96(3)}C_{60}$	79(5)	0.86(1)	0.588(9)	14.592(4)	776.8(5)	9 at 350	Cs_3C_{60}, Cs_4C_{60}
$Cs_{2.38}K_{0.62}C_{60}$ b1	$Cs_{2.28(2)}K_{0.72(2)}C_{60}$	87(1)	0.96(1)	0.659(6)	14.595(2)	777.3(3)	10 at 375	Cs_4C_{60}
$Cs_{2.38}K_{0.62}C_{60}$ b2	**$Cs_{2.36(2)}K_{0.64(2)}C_{60}$**	**88.0(6)**	**0.998(9)**	**0.681(5)**	**14.595(2)**	**777.3(3)**	**30 at 375**	**Cs_4C_{60}**
$Cs_{2.33}K_{0.67}C_{60}$ a[b]	**$Cs_{2.26(2)}K_{0.74(2)}C_{60}$**	**95(1)**	**0.91(1)**	**0.64(1)**	**14.6053(9)**	**778.9(1)**	**5 at 350**	**Cs_3C_{60}**
							7 at 450	
$Cs_{2.7}K_{0.3}C_{60}$	**$Cs_{2.32(2)}K_{0.69(2)}C_{60}$**	**68(1)**	**1.01(1)**	**0.656(9)**	**14.606(2)**	**779.0(1)**	**5 at 350**	**Cs_3C_{60}, Cs_4C_{60}**
$Cs_{2.68}Rb_{0.32}C_{60}$ a	**$Cs_{2.65(2)}Rb_{0.35(2)}C_{60}$**	**90(1)**	**0.982(4)**	**0.822(9)**	**14.6925(4)**	**792.92(7)**	**5 at 350**	**Cs_4C_{60}**
$Cs_{2.66}Rb_{0.34}C_{60}$ b1	**$Cs_{2.37(4)}Rb_{0.63(4)}C_{60}$**	**88(5)**	**0.87(2)**	**0.75(1)**	**14.679(1)**	**790.5(3)**	**13 at 400**	**Cs_3C_{60}, Cs_4C_{60}**
$Cs_{2.66}Rb_{0.34}C_{60}$ b2	$Cs_{2.37(4)}Rb_{0.63(4)}C_{60}$	83(3)	0.86(2)	0.756(9)	14.6892(6)	792.4(1)	17 at 400	Cs_3C_{60}, Cs_4C_{60}
$Cs_{2.66}Rb_{0.34}C_{60}$ c	$Cs_{2.10(6)}Rb_{0.90(6)}C_{60}$	79(3)	0.84(2)	0.63(2)	14.683(4)	791.4(5)	29 at 400	Cs_3C_{60}, Cs_4C_{60}
Cs_2RbC_{60}	**$Cs_{1.65(11)}Rb_{1.35(11)}C_{60}$**	**94(4)**	**0.87(5)**	**0.39(3)**	**14.586(5)**	**775.5(8)**	**13 at 375**	**Cs_4C_{60}**

(b) Superconducting Properties

sample	intragrain T_c, K^{-1}	intergrain T_c, K^{-1}	shielding fraction, %	transition width, K (10−50%)	V/C_{60}, Å^{-3}
$Cs_{2.26}K_{0.74}C_{60}$	30.1	28.1	50	4.2	773.2(1)
$Cs_{2.38}K_{0.62}C_{60}$ a1	29.5	28.1	40	4.5	775.0(1)
$Cs_{2.38}K_{0.62}C_{60}$ b2	27.8	27.0	30	5.4	777.3(3)
$Cs_{2.33}K_{0.67}C_{60}$ a[s]	29.1	27.4	40	5.0	778.9(1)
$Cs_{2.7}K_{0.3}C_{60}$	27.8	27.2	50	4.8	779.0(1)
$Cs_{2.66}Rb_{0.34}C_{60}$ b1	26.6	25.5	25	6.3	792.4(1)
$Cs_{2.68}Rb_{0.32}C_{60}$ a	27.0	24.6	60	4.3	792.92(7)
Cs_2RbC_{60}	31.0	28.0	40	6.4	775.5(8)

[a] Samples completely in boldface print appear in the Superconducting Properties part b. Potassium-doped samples are in the upper half and the rubidium-doped samples in the lower half of the table. The labels indicate a different sample (letter) and/or a different annealing (number). Consecutive annealings of the same sample are grouped together to show the effects of subsequent annealings. [b] Solid-state synthesis. [c] The intra- and intergrain T_c are defined in the text and the caption to Figure 5. The labels indicate a different sample (letter) and/or a different annealing (number) of a given composition, and correspond to those used in part a. The shielding fractions are derived from the zero field cooled dc magnetization at 5 K without correction for particle size. [d] O, octahedral; T, tetrahedral.

The reaction mixture was annealed at temperatures between 350 and 400 °C for several days as described in Table 1a. At this stage, magnetization, Raman, and powder X-ray diffraction data were recorded. The samples were then subjected to further annealings, which were monitored using the above techniques. $Cs_{2.68}Rb_{0.32}C_{60}$ exhibited no further change, but the potassium-containing samples did change upon annealing as shown in Table 1a. To investigate the influence of the synthetic route, $Cs_{2.7}Rb_{0.3}C_{60}$ and $Cs_{3-x}K_xC_{60}$ ($x = 0.62, 0.67$) samples were also synthesized by solid-state reaction of stoichiometric amounts of alkali metal with sublimed C_{60} in Pyrex tubes.

Powder X-ray Diffraction. Lattice parameters and phase purity were initially determined using a Siemens D5000 powder diffractometer (Cu Kα_1, 6° linear position-sensitive detector). Quantitative phase and structure analysis were performed using synchrotron X-ray data collected on station 9.1 of the Synchrotron Radiation Source at Daresbury Laboratory. The wavelength used was ∼1 Å, calibrated with a silicon standard. All samples were measured over 6−26° 2θ with a step size of 0.02° and step time of 2 s. Longer scans with increased angular range and step time were recorded for Rietveld analysis as detailed in the caption of Figure 1. The GSAS suite of programs were used for Rietveld refinement, with a pseudo-Voigt peak shape function and a shifted Chebyshev background function.

The C_{60}^{3-} anion was initially assumed to have the same size and geometry as in K_3C_{60},[13] and the coordinates were accordingly scaled to the lattice constant. In the case of the alkali metals, the refinement was started with alternating variation of the isotropic temperature factor and fractional occupancy of the octahedral and tetrahedral sites. In the final stages, these parameters could be refined simultaneously together with the positional and displacement parameters of the C atoms. Using only Cs on the metal sites and allowing the fractional occupancy to vary gave essentially the same electron count as using mixed occupancy. This provided an additional check for the stoichiometry in combination with the confirmation of a 3− charge from Raman spectroscopy.

Magnetic Measurements. Superconducting transition temperature determinations were performed using a Quantum Design MPMS5 SQUID magnetometer on ∼20-mg samples sealed in Pyrex ampules under reduced He pressure, with a 20-G measuring field, by cooling in zero field, measuring the ZFC magnetization on warming and the FC magnetization on cooling.

The zero field was determined experimentally by measuring the magnetic moment of the previously centered sample. A scan length of 6 cm was used routinely for the measurements.

The appearance of small positive magnetic moments on field cooling does not indicate the presence of the Wohlleben or paramagnetic Meissner effect,[14] but is an artifact of the SQUID used for the magnetic measurement. The variation of the remanent magnetic field with position inside the SQUID magnetometer is such that the remanent field at the center position of the scan is lower than at the turning points.[15] During cooling, the sample rests in the lowest position of the scan and consequently experiences a lower field during the scan.

More detailed magnetic measurements were undertaken on $Cs_{2.68}Rb_{0.32}C_{60}$ to estimate the critical current density J_c, the critical fields H_{c1} and H_{c2}, the coherence length ξ, and the penetration depth λ. The results of these measurements are presented in the Supporting Information as Figures S3 and S4.

Raman Spectroscopy. Raman measurements were carried out using a Dilor LABRAM spectrometer with a HeNe laser at 20-mW power

(13) Allen, K. M.; David, W. I. F.; Fox, J. M.; Ibberson, R. M.; Rosseinsky, M. J. *Chem. Mater.* **1995**, *7*, 764−770.

(14) Braunisch, W.; Knauf, N.; Kataev, V.; Neuhausen, S.; Grutz, A.; Kock, A.; Roden, B.; Khomskii, D.; Wohlleben, D. *Phys. Rev. Lett.* **1992**, *68*, 1908−1911.

(15) Blunt, F. J.; Perry, A. R.; Campbell, A. M.; Liu, R. S. *Physica C* **1991**, *175*, 539−544.

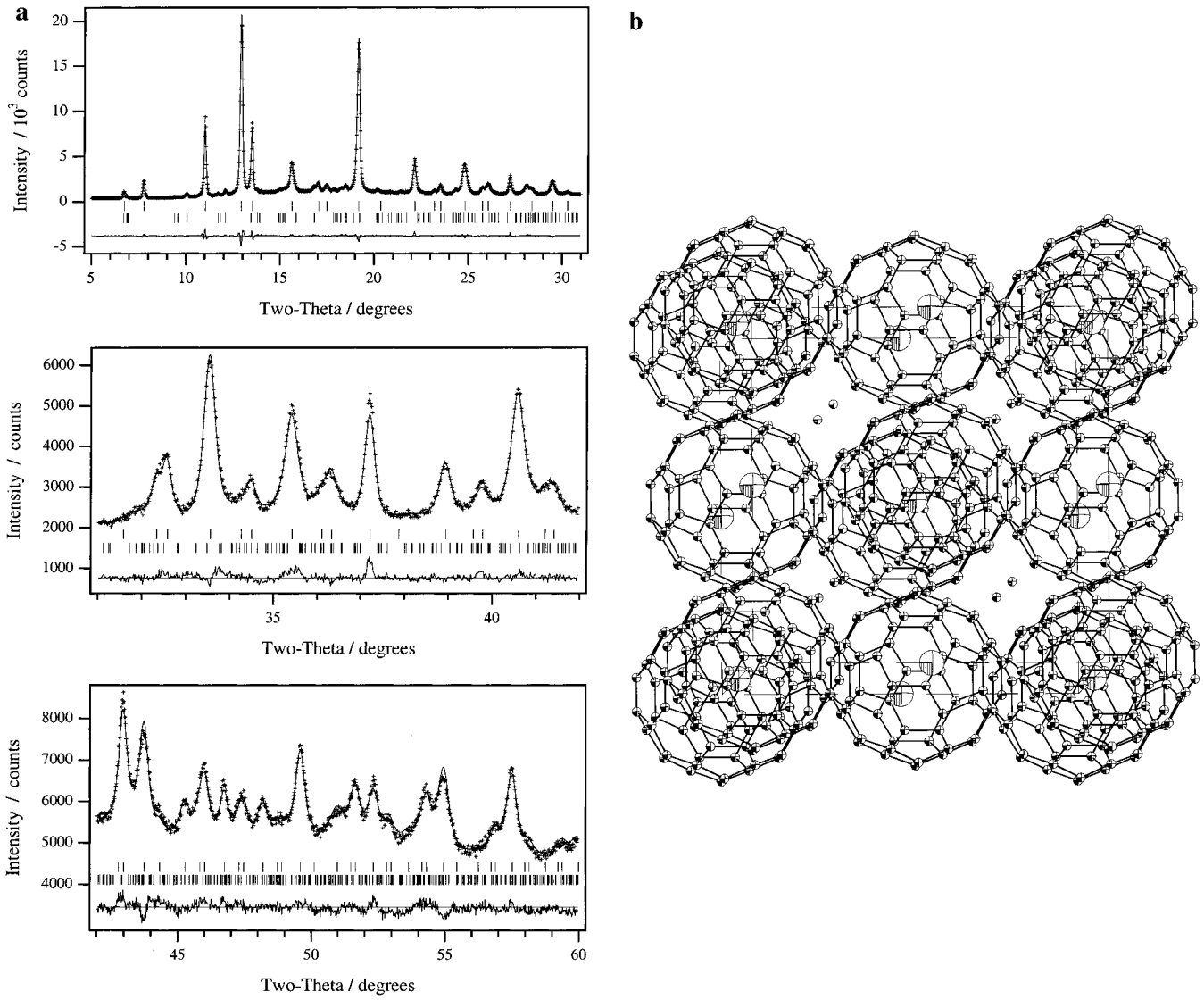

Figure 1. (a) Rietveld refinement of $Cs_{2.68}Rb_{0.32}C_{60}$ sample a. Data were collected on station 9.1 of the Daresbury Synchrotron Radiation Source and refined using the GSAS suite of programs. The occupancies of the octahedral and tetrahedral interstitial sites in the $Fm\bar{3}m$ symmetry phases are shown in Table 2 together with the refinement statistics. The step size was 0.02°, with steps of 6 s for 5−31°, 12 s for 31−42°, and 20 s for 42−60° 2θ, and the X-ray wavelength was 0.99503 Å. The refinement of $Cs_{2.68}Rb_{0.32}C_{60}$ (majority phase $Fm\bar{3}m$ $Cs_{2.65(2)}Rb_{0.35(2)}C_{60}$ $a = 14.6925(4)$ Å, 90(1)%) includes the *Immm* symmetry Cs_4C_{60} phase (lower tick marks, 10(1)%). (b) ORTEP representation of the structure of $Cs_{2.65(2)}Rb_{0.35(2)}C_{60}$. The fulleride anions are represented as orientationally ordered within space group $Fm\bar{3}$: the refined model in $Fm\bar{3}m$ contains two equally populated orientations related by a 90° rotation about the [001] direction. Thermal ellipsoids are represented at 50% probability. The octahedral site at the body center of the cell and equivalent positions is exclusively occupied by Cs^+.

with a wavelength of 632.817 nm. The measurements were made on the same glass capillaries used for the synchrotron experiments. The signal-to-noise ratio was limited by the fact that slow polymerization of the C_{60} was induced by the irradiation used.[16]

^{13}C MAS NMR. Solid-state MAS ^{13}C NMR measurements were carried out using a CMX Infinity spectrometer operating at a frequency of 50.3 MHz (4.7-T field). The samples were packed in Chemagnetics 7.5-mm-o.d. zirconia rotors for spinning in the Chemagnetics 200 APEX probe. Boron nitride plugs were used to seal the samples in the rotor. Typically ∼50 mg of sample was used and spun at 3.5 kHz. Chemical shifts are quoted relative to the ^{13}C shift of TMS by using adamantane as a secondary standard and are estimated to be reproducible within 0.5 ppm. To obtain isotropic values for the chemical shifts it was necessary to carry out NMR measurements at temperatures of up to 230 °C. The ^{13}C transverse magnetization was induced using a 4-μs radio frequency pulse and the free induction decay observed for 50 ms. A recycle delay of 100 ms was found to be sufficient to avoid saturation of the signals present.

Results

Recent work has indicated that care needs to be taken in removing all coordinated ammonia from rubidium fullerides prepared by the liquid ammonia route, with extended annealing above 350 °C required.[17] These problems are present but less severe in the case of the predominantly cesium-containing phases which are the subject of the present study. From weight analysis, the composition of the product recovered from liquid ammonia in the synthesis of $Cs_{2.7}Rb_{0.3}C_{60}$ could be determined as $Cs_{2.7}Rb_{0.3}C_{60}$·0.4(1) NH_3. CHN analysis of the final product is consistent with the complete removal of ammonia during the 6-h treatment at 120 °C (before deammoniation C 61.66(2)%, H 1.42(6)%, N 0.4%; after deammoniation C 63.0(6)%, H 0.7-(2)%, N 0.0%. For $Cs_{2.7}Rb_{0.3}C_{60}$ C_{calc} 65.21%). (The annealed phase had phase fractions of 64(1)% fcc, $a = 14.685(3)$ Å, 22% *Immm* and 15% $Pm3n$ Cs_3C_{60} impurity, $T_c = 27$ K, shielding

(16) Dresselhaus, M.; Dresselhaus, G.; Eklund, P. *J. Raman Spectrosc.* **1996**, *27*, 351−371.

(17) Chen, X.; Maniwa, Y.; Muroga, N.; Glenis, S.; Lin, C.; Labes, M. *Chem. Mater.* **1998**, *10*, 503−508.

Table 2. Refinement Statistics for $Cs_{2.68}Rb_{0.32}C_{60}$ a $\chi^2 = 3.080$, 90(1)% *Fm*3*m*, $a = 14.6925(4)$ Å, Refined Stoichiometry $Cs_{2.65(2)}Rb_{0.35(2)}C_{60}$. 10(1)% *Immm*, $a = 12.171(6)$ Å, $b = 11.968(5)$ Å, $c = 11.397(4)$ Å, Refined Stoichiometry $Cs_{3.96(6)}C_{60}$

histogram	R_w	R_e	R_f
1	0.0505	0.0257	0.0161
2	0.0280	0.0180	0.0096
3	0.0196	0.0131	0.0288

Phase Details for *Fm*$\bar{3}$*m* $Cs_{2.65(2)}Rb_{0.35(2)}C_{60}$:

	x	*y*	*z*	occupancy	U_{iso},Å^2
C(1)	0.0	0.0477(1)	0.2399(5)	0.5	0.015(1)
C(2)	0.2053(3)	0.0813(2)	0.0918(2)	0.5	0.015(1)
C(3)	0.1736(3)	0.1605(2)	0.0494(1)	0.5	0.015(1)
Cs(1)	0.5	0.5	0.5	0.982(4)	0.111(1)
Rb(1)	0.5	0.5	0.5	0.018(4)	0.111(1)
Cs(2)	0.25	0.25	0.25	0.822(9)	0.014(1)
Rb(2)	0.25	0.25	0.25	0.178(9)	0.014(1)

Selected Bond Lengths (Å) for the *Fm*$\bar{3}$*m* $Cs_{2.65(2)}Rb_{0.35(2)}C_{60}$ Majority Phase in $Cs_{2.68}Rb_{0.32}C_{60}$ Sample a[a]

C(1)	C(1)	1.401(2)	Cs/Rb(2)	C(3)	3.417(2)
C(2)	C(3)	1.400(2)	Cs/Rb(2)	C(2)	3.461(4)
C(1)	C(2)	1.451(1)	Cs(1)	C(1)	3.885(7)
C(2)	C(3)	1.449(3)			
C(3)	C(3)	1.452(2)			

[a] For this refinement, soft constraints on the bond lengths were used: single bond 1.400(1) Å and double bond 1.450(1) Å. The mean angles for the five- and six-membered rings are 108.3° (105.42−110.68°) and 119.4° (116.50−126.87°), respectively. The mean radius of the C_{60} molecule is 3.38 Å, and the maximum deviation from this value is smaller than 0.05 Å.

fraction 15%). This liquid ammonia route has previously been used to prepare ammonia-free Cs_4C_{60}.[18]

Rietveld refinement of the synchrotron X-ray powder diffraction data shows quantitatively that the samples prepared by the liquid ammonia route contain at least 70% of an fcc phase with the *Fm*$\bar{3}$*m* merohedrally disordered structure of K_3C_{60}[19] (Figure 1a and Table 1a). Figures 1 and S1 show Rietveld refinements of samples of nominal composition of $Cs_{2.68}Rb_{0.32}C_{60}$ and $Cs_{2.66}Rb_{0.34}C_{60}$. The data on $Cs_{2.68}Rb_{0.32}C_{60}$ were collected with a variable counting time strategy to allow accurate evaluation of the intensities of the high-angle reflections and permit precise refinement of the C_{60}^{3-} molecular geometry and the cation site occupancies. The bond lengths and angles reported in Table 2 are consistent with reported C_{60}^{3-} geometries,[13] indicating the quality of the refinement, which proves the successful synthesis of the largest lattice parameter fcc fulleride yet reported. The structure of the fcc phase $Cs_{2.65(2)}Rb_{0.35(2)}C_{60}$, the fcc phase in the $Cs_{2.68}Rb_{0.32}C_{60}$ sample, is represented in Figure 1b.

Small quantities of A_4C_{60}, Cs_3C_{60} and cubic A_1C_{60} impurities coexist in all the samples we have prepared (Table 1a). None of these impurities are superconducting at ambient pressure. For the A_4C_{60} phase, the *Immm* model with A = Cs was used.[18] The small variations in the lattice parameters of this impurity phase ($12.14(1) \le a/\text{Å} \le 12.198(2)$, $11.889(2) \le b/\text{Å} \le 11.968(6)$, $11.397(4) \le c/\text{Å} \le 11.448(6)$) about the parameters for pure Cs_4C_{60} ($a = 12.1496(9)$ Å, $b = 11.9051(9)$ Å, $c = 11.4520(9)$ Å), synthesized under the same conditions as the samples prepared in liquid ammonia, and the similarity of the unit cell volumes ($1650 \le V \le 1663$ Å^3, $V = 1656.4(3)$ Å) suggest that deviations in total cation concentration from 4 and substitution of K^+ and Rb^+ for Cs^+ are small in the *Immm* phases. Cs_3C_{60}, in which superconductivity is only observed under applied pressure,[4] can be prepared either in the *Pm*$\bar{3}$*n* A15 structure or isostructural with Cs_4C_{60} with very similar lattice constants and unit cell volume (1659(2) Å^3).[20] Attempts to include second fcc A_3C_{60} phases with smaller lattice parameters into the fit were either unsuccessful or lead to very small phase fractions, e.g., for $Cs_{2.38}K_{0.62}C_{60}$ 0.5(4)% of an $a = 14.391(4)$ Å A_3C_{60} phase could be included in the refinement.

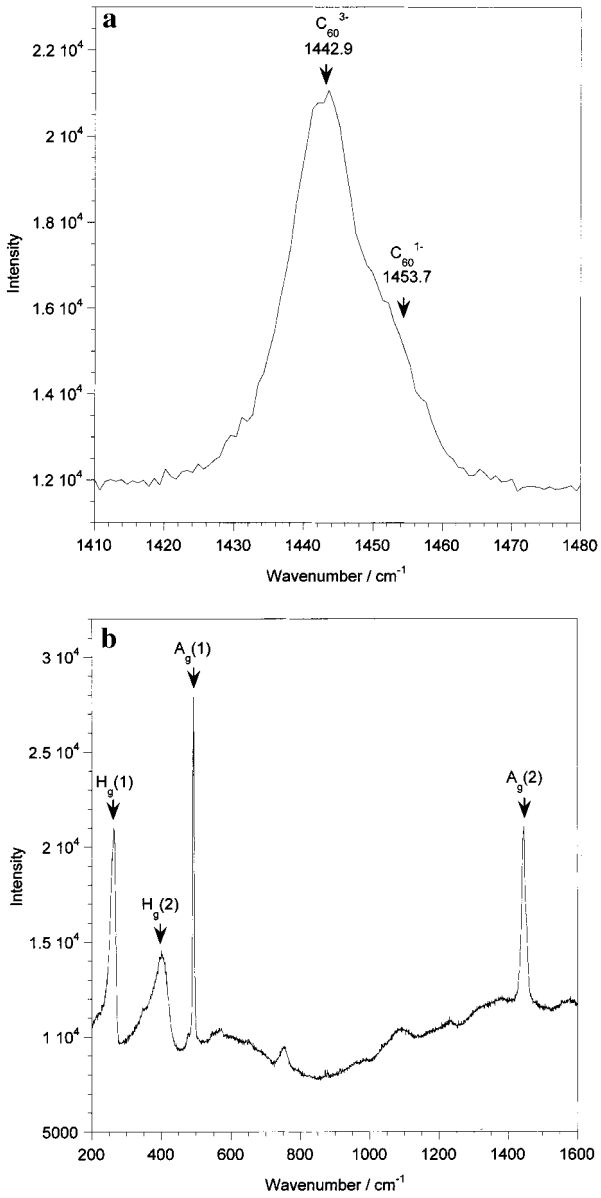

Figure 2. Raman data on $Cs_{2.38}K_{0.62}C_{60}$ (sample a1) after annealing at 350 °C for 12 days. (a) The $A_g(2)$ Raman modes for the two phases present (A_3C_{60} (1442.9 cm^1) and A_1C_{60} (1453.7 cm^{-1}) with respective fractions of 72 and 28% from Rietveld refinement (Table 1a)). (b) The observed frequencies of the other observed modes in the A_3C_{60} phase are $H_g(1)$ 246 cm^{-1}, $H_g(2)$ 401 cm^{-1}, $H_g(4)$ 752 cm^{-1}, and $A_g(1)$ 492 cm^{-1}.

Raman and MAS NMR measurements are consistent with the phase identification from the quantitative treatment of the X-ray data. Figure 2b shows Raman spectra of $Cs_{2.38}K_{0.62}C_{60}$ after annealing at 350 °C for 29 days. The $A_g(2)$ mode (Figure 2a) of the majority phase is at 1445 cm^{-1} (15 cm^{-1} fwhm),

(18) Dahlke, P.; Henry, P. F.; Rosseinsky, M. J. *J. Mater. Chem.* **1998**, *8*, 1571−1576.

(19) Stephens, P. W.; Mihaly, L.; Lee, P. L.; Whetten, R. L.; Huang, S.-M.; Kaner, R.; Diederich, F.; Holczer, K. *Nature* **1991**, *351*, 632−634.

(20) Yoshida, Y.; Kubozono, Y.; Kashino, S.; Murakami, Y. *Chem. Phys. Lett.* **1998**, *291*, 31−36.

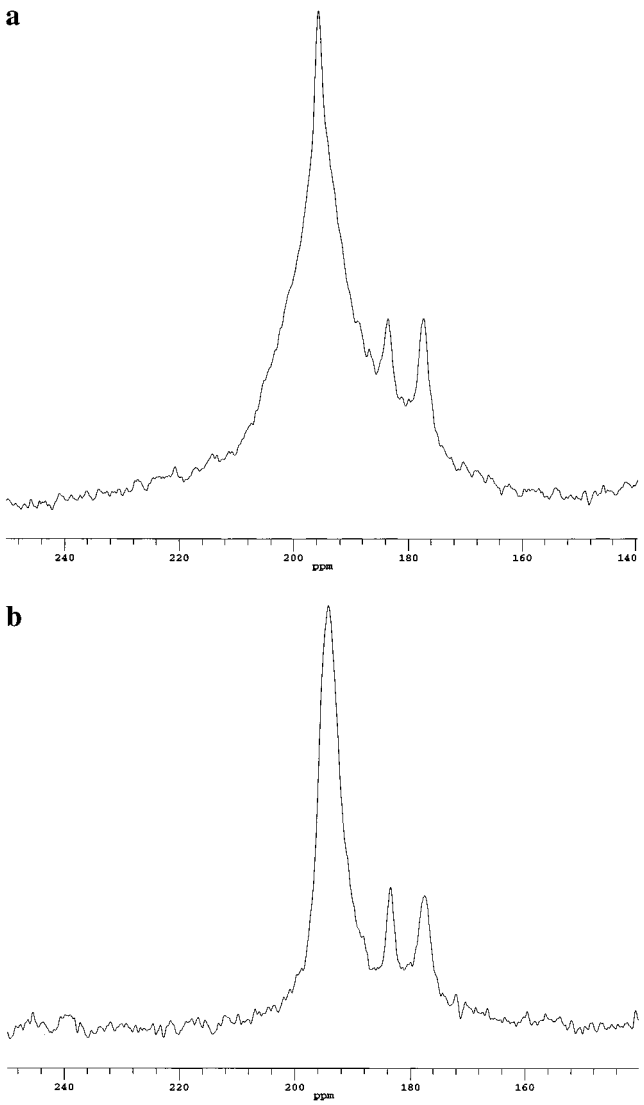

Figure 3. ^{13}C MAS NMR spectra of (a) $Cs_{2.68}Rb_{0.32}C_{60}$ and (b) $Cs_{2.38}K_{0.62}C_{60}$ a3 at 230 °C. The isotropic ^{13}C chemical shift of $Cs_{2.38}K_{0.62}C_{60}$ is 194.9 ppm. The minority resonances correspond to A_1C_{60} and A_4C_{60} impurity phases.

which clearly indicates a charge state of C_{60}^{3-},[21,22] with a small quantity of C_{60}^{-1} impurity indicated by the $A_g(2)$ frequency at 1455 cm^{-1} (7% of the total $A_g(2)$ peak area). The frequencies assigned to the $A_g(2)$ mode of C_{60}^{3-} are observed at 1444.5 ± 2 cm^{-1} in all the samples. In the samples where the powder diffraction data indicated an A_4C_{60} impurity, a minority $A_g(2)$ mode was observed at 1440 cm^{-1}. ^{13}C MAS NMR measurements at 230 °C revealed, in addition to the dominant resonance at around 195 ppm from the C_{60}^{3-} phase, sharp resonances at 183.8 and 177.6 ppm, consistent with minority A_4C_{60} and cubic A_1C_{60} phases (Figure 3).

The Raman, NMR, and X-ray data demonstrate that the majority component of the $Cs_{3-x}A_xC_{60}$ samples prepared by the liquid ammonia route are fcc phases with C_{60}^{3-} charges and the largest lattice parameters yet demonstrated in the A_3C_{60} family.

Once formed, the expanded fcc phases are stable to annealing at temperatures of up to 450 °C as shown by the data for sample $Cs_{2.33}K_{0.67}C_{60}$ a in Table 1a. Annealing at higher temperatures lead to the disproportionation of $Cs_{2.38}K_{0.62}C_{60}$ into the more stable A_4C_{60} and A_1C_{60} phases.

Synthesis by the conventional solid−vapor reaction affords smaller phase fractions of expanded fcc fullerides than the liquid ammonia route, and the composition range over which expanded fcc phases can be prepared is narrower. The nominal composition $Cs_{2.33}K_{0.67}C_{60}$ when prepared by the solid−vapor route produces an fcc phase fraction of 95(1)%, while $Cs_{2.38}K_{0.62}C_{60}$ when prepared by the same route only forms 9(1)% of an fcc phase with a = 14.612(5) Å. The attempted solid−vapor preparation of $Cs_{2.7}Rb_{0.3}C_{60}$ resulted only in 13(4)% fcc phase fraction with a refined composition $Cs_{2.45(7)}Rb_{0.55(7)}C_{60}$ and a = 14.672(1) Å. It is important to note that the properties of $Cs_{2.33}K_{0.67}C_{60}$ prepared by a solid-state route, which has the same intrinsic intragrain T_c as the $Cs_{2.7}K_{0.3}C_{60}$ prepared from liquid ammonia with very similar lattice parameters, are consistent with the absence of ammonia in the solution-prepared samples (Table 1).

The multiphase Rietveld refinements reveal the lattice parameters and structural details of the large a fcc phases. The larger cesium cations preferentially occupy the octahedral site. The isotropic temperature factors for the cation sites refined typically as 0.10(1) $Å^2$ for the octahedral and 0.01(1) $Å^2$ for the tetrahedral site, reflecting the relative sizes of these interstices. The extent of cation ordering and the actual composition of the fcc component are shown in Table 1a to depend on the precise synthesis route. $Cs_{2.38}K_{0.62}C_{60}$ was subjected to longer annealing periods at 350 °C and shows an increase of lattice parameter with heating time (Table 1a), due to reaction with cesium-containing A_1C_{60} and A_4C_{60} impurities produced in the initial liquid ammonia synthesis. The fcc phase fraction increases from 72(1) to 100%. The influence of cation order on the lattice parameter is shown by the subsequent reduction of a to 14.6276(9) Å for the same sample after 7 days at 350 °C due to the smaller fraction of Cs^+ on the tetrahedral site (Table 1a).

The largest lattice parameter a = 14.6925(4) Å phase with the nominal composition $Cs_{2.68}Rb_{0.32}C_{60}$ refines to have a composition $Cs_{2.65(2)}Rb_{0.35(2)}C_{60}$, with the Rb^+ cations confined to the tetrahedral sites (Table 1a). Reducing the rubidium content of the $Cs_{3-x}Rb_xC_{60}$ phase below x = 0.32 in order to achieve an even larger inter-fulleride separation led only to smaller phase fractions of the fcc phase and to no increase of the unit cell volume of the fcc phase. An example is $Cs_{2.7}Rb_{0.3}C_{60}$ for which CHN analysis was undertaken at several stages of its preparation as reported earlier in the paper. The final product had a = 14.685(3) Å for the fcc phase with a phase fraction of 64(1)% (22% *Immm* and 15% *Pm*3*n* phases).

The fcc lattice parameter increases as expected with Cs concentration, but it is the Cs concentration on the tetrahedral site rather than the overall value that determines the lattice parameter variation in both the K- and Rb-substituted families (Figure 4). The rate of increase $\partial a/\partial f_{Cs(tet)}$ is larger in the $Cs_{3-x}K_xC_{60}$ than the $Cs_{3-x}Rb_xC_{60}$ series because the tetrahedral cation at the Cs_2MC_{60} composition is smaller, and thus an increase in the cesium concentration on the tetrahedral site has a more pronounced effect on the lattice parameter. As well as demonstrating the consistency of the refined site occupancies, Figure 4 allows a reliable extrapolation to the lattice constant of the hypothetical fcc Cs_3C_{60} as 14.76 Å (V/C_{60}= 804 $Å^3$), which is the convergence of the Vegard's law plots for both families. This structure would have octahedral vacancies with

(21) Mitch, M. G.; Lannin, J. S. *Phys. Rev. B* **1995**, *51*, 6784.
(22) Winter, J.; Kuzmany, H. *Solid State Commun.* **1992**, *84*, 935.

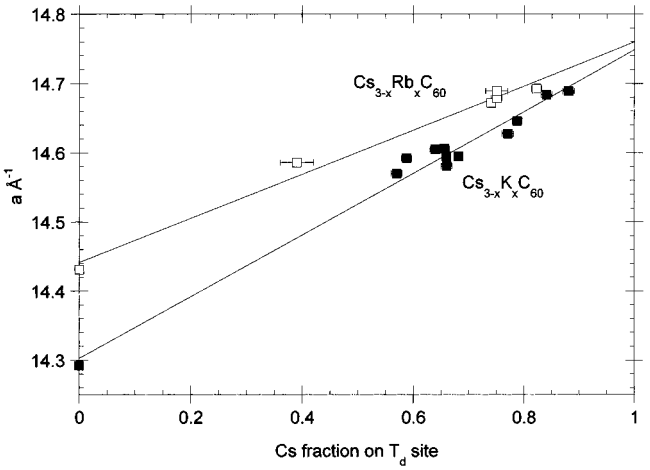

Figure 4. Lattice parameter of $Cs_{3-x}A_xC_{60}$ (A = K, Rb) phases determined by cesium occupation of the tetrahedral site according to Vegard's law.

a radius of 2.37 Å (calculated with a van der Waals radius of 5.01 Å for C_{60}^{3-}[23]), much larger than the ionic radius of Cs^+ of 1.70 Å. Orthorhombic Cs_3C_{60} is reported to form an even less dense packing with V/C_{60}= 830(1) Å^3, while the *Pm*3*n* A15 structure phase has a volume of 815 Å^3/C_{60}.

The magnetization measurements show that the new large lattice parameter phases are bulk superconductors.(Figure 5; Table 1b) The shielding fractions in Table 1b are not corrected for particle size[24] and therefore represent a lower limit, which is ≥25% for all samples prepared via the liquid ammonia route. Contrary to the predictions of all existing $T_c(a)$ relationships for A_3C_{60} fullerides, T_c decreases as the size of the fcc unit cell increases; e.g., $Cs_{2.68}Rb_{0.32}C_{60}$ has a lower transition temperature than $Cs_{2.26}K_{0.74}C_{60}$ (Figure 5a). This apparent variation in T_c with a has to be treated with caution due to the existence of other possible explanations for the suppression of T_c. Screening currents in separate grains (intragrain contribution) and screening currents in clusters formed by several grains (intergrain contribution) constitute the diamagnetic moment of the superconducting powder.[25]

Josephson-type links between the superconducting phase and a second phase can lead to a decrease in T_c.[26] Possible candidates for this SN or proximity effect are the A_1C_{60} and A_4C_{60} impurity phases. To verify that this effect was not responsible for the reduction of T_c in the ternary phases, reference samples were investigated. Grinding together Rb_3C_{60} and Cs_4C_{60} in a 1:1 molar ratio does not have any effect on the superconducting transition temperature (T_c = 29 K) of Rb_3C_{60} (Figure 6a).

A sample of nominal composition $Rb_{3.3}C_{60}$ ($0.7Rb_3C_{60}$ + $0.3Rb_4C_{60}$) was prepared by the liquid ammonia route used for the ternary phases. After 8 days annealing at 350 °C, a single diamagnetic transition at T_c = 26.9(5) K was observed. Fischer et al.[27] found no effect of Rb_4C_{60} on the T_c of Rb_3C_{60} in a sample with the nominal composition $Rb_{3.17}C_{60}$, but observed a decrease of the shielding fraction when departing from the ideal stoichiometry. After further annealing of the liquid ammonia sample

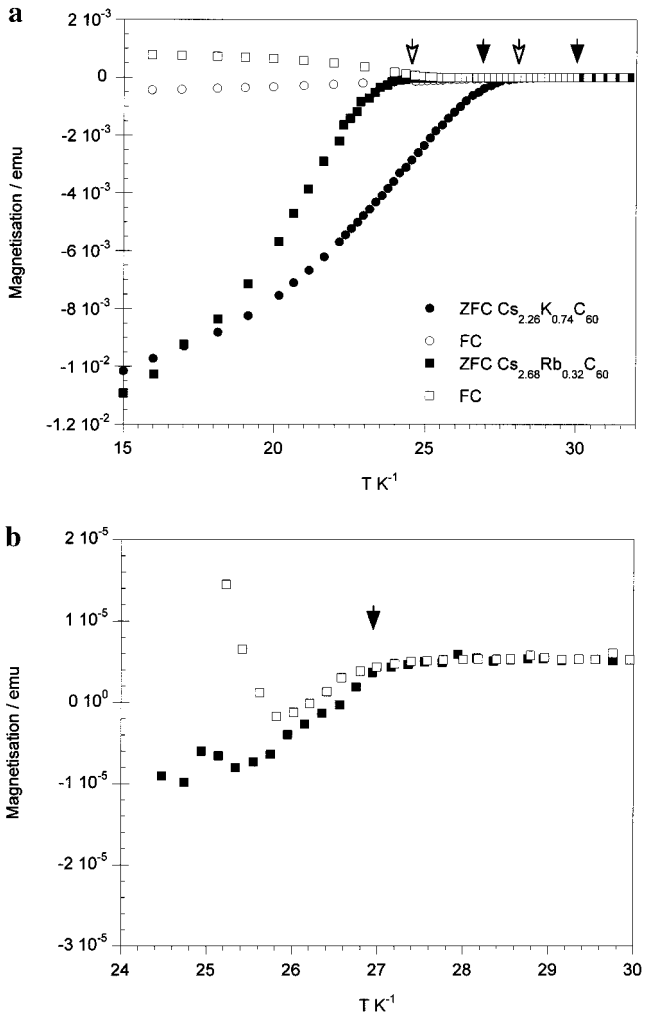

Figure 5. (a) Temperature dependence of the magnetic dc susceptibility for $Cs_{2.26}K_{0.74}C_{60}$ (92(1)% fcc phase fraction, a = 14.570(1) Å) (circles) and $Cs_{2.68}Rb_{0.32}C_{60}$ (90(1)% fcc phase fraction, a = 14.6925(4) Å) (squares) at H = 20 G. Zero-field cooled (ZFC) data (collected on warming) and field cooled (FC) data (collected on cooling) are shown as filled and open symbols, respectively. The diamagnetic moment arises from field exclusion (ZFC) and expulsion (FC) due to spontaneous electric currents in the superconducting state. The arrows indicate the transition temperatures T_c. The filled arrows represent the intrinsic intragrain T_c. The open arrows show the onset of the superconducting fraction with large shielding, attributed to intergrain coupling. (b) The expanded temperature scale shows the small shielding fraction corresponding to the intrinsic intragrain T_c of $Cs_{2.68}Rb_{0.32}C_{60}$.

of $Rb_{3.3}C_{60}$ (20 days at 400 °C), it was possible to detect two superconducting transitions, one at 29 K with a very small shielding fraction (Figure 6b) and a second at 26.5 K (Figure 6a). The transition at higher temperature corresponds to the expected value for Rb_3C_{60} and shows the onset of superconductivity in individual grains. The transitions can be separately attributed to intra- and intergrain coupling. Irregularly shaped particles with sizes not much larger than the penetration depths (λ = 3100 Å for $Cs_{2.68}Rb_{0.32}C_{60}$) will show very small shielding fractions,[28] as observed for the upper "correct" transition temperature. The grain size before this additional annealing was not large enough to show this effect. This has been observed for Rb_3C_{60}/Na_xC_{60}[26] mixtures and is assigned to a small grain size for the superconducting phase giving rise to a diamagnetic response dominated by intergrain coupling.

(23) Murphy, D. W.; Rosseinsky, M. J.; Fleming, R. M.; Tycko, R.; Ramirez, A. P.; Haddon, R. C.; Siegrist, T.; Dabbagh, G.; Tully, J. C.; Walstedt, R. E. *J. Phys. Chem. Solids* **1992**, *53*, 1321.

(24) Schoenberg, D. *Proc. R.Soc. (London)* **1949**, *A175*, 49.

(25) Neminsky, A.; Shovkun, D.; Vyaselev, O. *Phys. Rev. B* **1996**, ***54***, 454.

(26) Glenis, S.; Cooke, S.; Chen, X.; Labes, M. *Mol. Cryst. Liq. Cryst. Sci. Technol., Sect. A* **1996**, *284*, 139−147.

(27) Fischer, J. E.; Bendele, G.; Dinnebier, R.; Stephens, P. W.; Lin, C. L.; Bykovetz, N.; Zhu, Q. *J. Phys. Chem. Solids* **1995**, *56*, 1445−1457.

(28) Buntar, V.; Weber, H. W. *Supercond. Sci. Technol.* **1996**, *9*, 599−615.

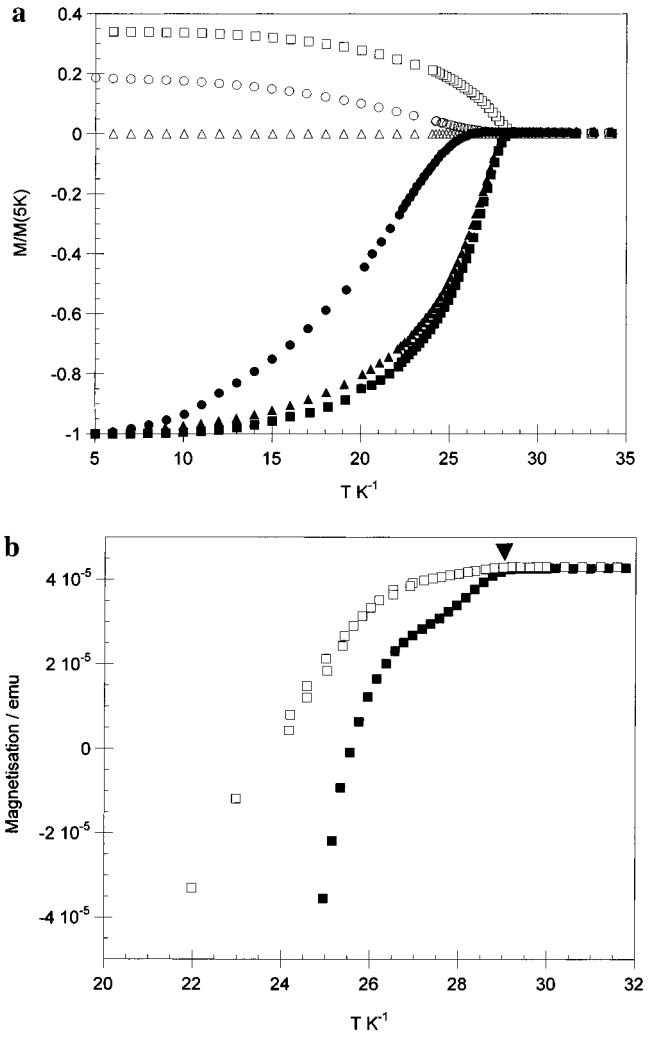

Figure 6. (a) Temperature dependence of the magnetic dc susceptibility of Rb_3C_{60} (squares; prepared by solid−vapor reaction), $Rb_{3.3}C_{60}$ (circles; prepared by liquid ammonia synthesis and annealed as described in the text), and a mechanical mixture of Rb_3C_{60} and Cs_4C_{60} (triangles). ZFC data (collected on warming) and FC data (collected on cooling) are shown as filled and open symbols, respectively. The data for all three compounds have been normalized to their 5 K value. (b) The onset of superconductivity at $T = 29.0$ K with a very small shielding fraction is observed for the annealed $Rb_{3.3}C_{60}$ sample prepared by the liquid ammonia route. This corresponds to the intrinsic intragrain T_c, indicated by the arrowhead.

The magnetization data on the liquid ammonia-derived expanded A_3C_{60} phases can now be considered in the light of the above studies. The ternary samples were heated for periods of between 5 and 76 days at temperatures of 350−450 °C. Critical temperatures with very small shielding fractions, which lie above the apparent critical temperatures observed without magnification of the data, are indicated by the filled arrows in Figure 5a. We attribute these higher transition temperatures, shown in more detail in Figure 5b, to the onset of intragrain coupling. The intergrain coupling with a larger shielding fraction (see Table 1b) is then observable at lower temperature. The above studies lead us to identify the higher temperature transition (Figure 5b) with the intrinsic transition in the expanded A_3C_{60} phases. This interpretation gives a less dramatic suppression of T_c with increasing lattice parameter. Superconducting transition temperatures are reported in Table 1b and shown as a function of volume per C_{60}^{3-} anion in Figure 7. The ZFC shielding fractions are all consistent with bulk superconductivity from

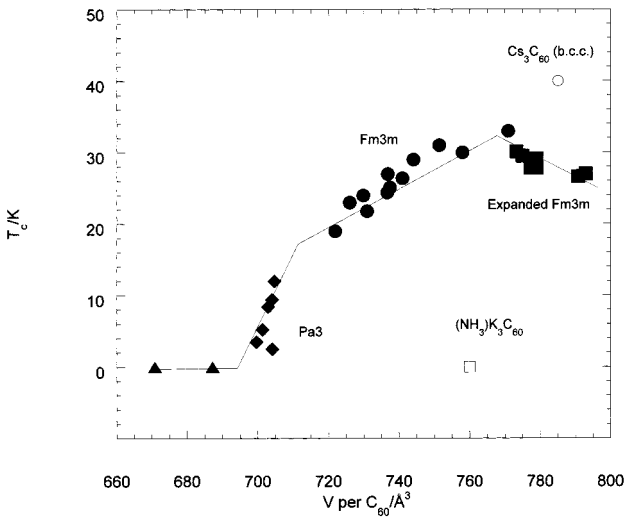

Figure 7. Effect of volume per C_{60}^{3-} anion on the electronic properties of A_3C_{60} fullerides. The filled squares represent the intrinsic intragrain superconducting transition temperatures of the expanded fcc phases. The filled circles show the dependence of T_c on the volume per C_{60}^{3-} anion as described in the literature[1] for $Fm\bar{3}m$ A_3C_{60} phases with smaller unit cell volumes and the diamonds are for Na_2AC_{60} with the $Pa\bar{3}$ structure, bcc Cs_3C_{60} ($T_c = 40$ K), and tetragonal $(NH_3)K_3C_{60}$, which undergoes a metal insulator transition at 40 K, are also shown.[1]

the fcc phase in a powder sample. All samples show Meissner fractions (expulsion of magnetic field upon field cooling) close to zero. This indicates very strong flux pinning, probably due to a large abundance of defects or disorder. Correspondingly, the X-ray Rietveld refinements improved significantly with the introduction of Lorentzian Scherrer broadening with ⟨111⟩ taken as the anisotropic broadening axis. Anomalous broadening of $h \neq k \neq l$ reflections owing to stacking faults between the close-packed (111) planes has also been reported for Rb_3C_{60} prepared by solid-state methods.[27]

The maximum T_c observed in the new family never exceeds 31 K. This indicates that the $T_c(a)$ relationship has either reached a plateau or passed through a maximum. This is consistent with the significantly lower $\partial T_c/\partial a$ dependence of Rb_2CsC_{60} compared to Rb_3C_{60} revealed by the pressure dependence of T_c.[16] A negative $\partial T_c/\partial a$ dependence has previously been reported in the pressure dependence of superconductivity in Ca_5C_{60}[29] and in the $A_3Ba_3C_{60}$ (A = K, Rb, Cs) series[30] where the density of states measured by dc magnetization decreases with increasing lattice parameter.

The polyphasic nature of the present materials makes direct measurement of $N(E_f)$ with a bulk probe such as dc susceptibility impossible, but the local ^{13}C MAS NMR technique is able to resolve the phases and give information on $N(E_f)$ in the A_3C_{60} phase via the total shift. At room temperature, broad ^{13}C signals are observed from all the large lattice parameter phases studied, similarly to those found for Rb_3C_{60}[11], but warming to 230 °C results in pronounced motional narrowing and a sharp single-resonance characteristic of anions reorienting rapidly on the NMR time scale (Figure 3). The observed shifts are consistent with but slightly lower than extrapolation from existing shift−lattice parameter relationships. The extrapolated isotropic shift[11] is 196 ppm for 14.6 Å and 199 ppm for 14.7 Å. For $Cs_{2.68}Rb_{0.32}C_{60}$ ($a = 14.6925(4)$ Å), the isotropic ^{13}C shift is 196.0 ppm at 230 °C (Figure 3a).

(29) Schirber, J. E.; Bayless, W. R.; Kortan, A. R.; Kopylov, N. *Physica C* **1993**, *213*, 190.
(30) Iwasa, Y.; Kawaguchi, M.; Iwasaki, H.; Mitani, T.; Wada, N.; Hasegawa, T. *Phys. Rev. B* **1998**, *57*, 13395−13398.

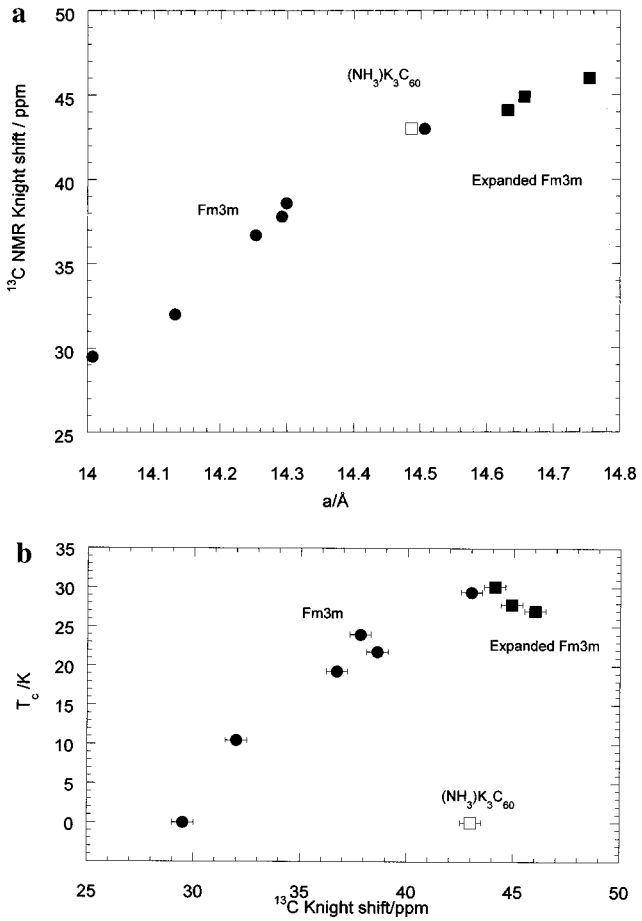

Figure 8. (a) Variation of ^{13}C Knight shift with lattice parameter in the A_3C_{60} series. Expanded phases are shown with filled symbols. Data for the $Fm\bar{3}m$ A_3C_{60} and $(NH_3)K_3C_{60}$ points are taken from ref 11 and the lattice parameters of the expanded phases are computed at 230 °C from the expansion coefficient (d ln a/dT) = 3×10^{-5} K^{-1}.[39] (b) Variation of superconducting transition temperature with ^{13}C Knight shift in fcc A_3C_{60} phases.

The isotropic NMR shift δ is the sum of the isotropic chemical shift σ and the Knight shift K. The isotropic chemical shift σ is assumed to be constant for all the A_3C_{60} phases. An appropriate although not undisputed value is 150 ppm.[11,31] Other values reported are 180[32] and 125 ppm.[33] The 150 ppm value is in close agreement with the NMR shift δ of C_{60} (143 ppm) plus a correction of 8 ppm due to the charge,[34] and we choose this value here (the EPR-derived $\chi_{Pauli} = 6 \times 10^{-4}$ emu mol^{-1} for K_3C_{60} yields a predicted Knight shift $K_{iso} = \chi_{Pauli}/(1.73 \times 10^{-5}) = 34$ ppm, so the total shift of 186 ppm yields $\sigma = 152$ ppm, in good agreement with this assumption). The density of states at the Fermi level can be derived from the Knight shift using $N(E_F) = 0.27\ K_{iso}$ (states/eV C_{60} spin).[11] This gives 11.9 $< N(E_f)$/(states/eV C_{60} spin) < 12.4 for the new expanded fcc phases.

Figure 8a shows the variation of Knight shift with lattice parameter, while the dependence of T_c on Knight shift is given in Figure 8b. These data show that when the A_3C_{60} lattice parameter is larger than 14.555 Å T_c decreases with increasing lattice constant, but the transition temperature is now no longer proportional to the Knight shift. It is important to note that the normal state properties of the expanded A_3C_{60} phases are consistent with those of previously studied smaller lattice parameter A_3C_{60} phases in that the measured $N(E_f)$ increases upon expansion. It is the suppression of T_c upon expansion, demonstrated by the reversal of the expected dependence of T_c upon Knight shift for the large lattice parameter phases, that is unconventional.

Discussion

The fcc phases with large cesium concentrations in the A_3C_{60} family reported here are metastable phases with the largest lattice parameters yet found in this series. The Raman data demonstrate that the anion charges are the same as those found in K_3C_{60} and other members of the family. These composition ranges have been previously studied, but superconducting volume fractions were low and importantly the superconducting phase, and its structure, were not identified.[35] The liquid ammonia synthesis route avoids the initial formation of the stable A_1C_{60} and A_4C_{60} phases, which occurs in higher temperature reactions, giving high superconducting volume fractions and fcc phase fractions that allow identification of the superconducting phase as a large a fcc A_3C_{60} system. The solid-state/vapor diffusion route is successful in preparing large phase fractions of fcc materials when the target phase has a lattice parameter of less than 14.60 Å, but gives very small fcc phase fractions for more cesium-rich compositions.

Within this family, an increase in fcc lattice parameter beyond 14.555 Å [3] ($RbCs_2C_{60}$, $T_c = 33$ K) fundamentally changes the dependence of the electronic properties on inter-fulleride separation. The present measurements allow us to define the electronic phase diagram for C_{60}^{3-} fullerides at the large inter-fulleride separations where the superconducting transition temperatures are highest. The information that can be derived from the normal state properties is discussed before an analysis of the superconducting behavior. The interpretation of the normal state properties of metallic A_3C_{60} fullerides is complex because they are narrow-band metals: the t_{1u} bandwidth W is comparable with the on-site interelectron repulsion U, as well as several intramolecular energies arising from Jahn−Teller electron−phonon coupling and multiplet splitting.[1,36] The bandwidth W represents the lowering of the electrons kinetic energy by delocalization into itinerant states, favoring metallic behavior in a partially filled band and leading to the well-known prediction of simple band theory that all solids with partially filled bands are metallic. The observation that this is not the case when W is small (e.g., the transition metal oxide NiO has a partially filled 3d band but is an insulator) leads to the development of the Hubbard model, in which the interelectron repulsion between two electrons occupying the same site in the solid (U) opposes the delocalization of the electrons and favors their localization as discrete spins on individual sites.[37] The on-site repulsion U in A_3C_{60} is ∼1 eV, while the bandwidth depends on the details of the local orientations of the C_{60}^{3-} anions, but estimates at the inter-fulleride separation appropriate to Rb_3C_{60} and K_3C_{60} are between 0.5 and 0.6 eV, giving U/W of between 1.25 and 2.6.[36] The single-band Hubbard model is predicted to be insulating at this point, but the orbital degeneracy in the Hubbard model for C_{60}^{3-} phases increases the critical value of

(31) Zimmer, G.; Helmle, M.; Mehring, M.; Rachdi, F.; Reichenbach, J.; Firlej, L.; Bernier, P. *Europhys. Lett.* **1993**, *24*, 59−64.
(32) Chen, J.; Sha, Q. F.; Cai, R. F.; Huang, Z. E. *Solid State Commun.* **1996**, *96*, 199.
(33) Kerkoud, R.; Auban-Senzier, P.; Jerome, D.; Lambert, J. M.; Zahab, A.; Bernier, P. *Europhys. Lett.* **1994**, *25*, 379−384.
(34) Spiesecke, H.; Schneider, W. G. *Tetrahedron Lett.* **1961**, *14*, 486.
(35) Tanigaki, K.; Hirosawa, I.; Mizuki, J.; Ebbesen, T. W. *Chem. Phys. Lett.* **1993**, *213*, 395.
(36) Gunnarsson, O. *Rev. Mod. Phys.* **1997**, *69*, 575−606.
(37) Cox, P. A. *The Electronic Structure and Chemistry of Solids*; Oxford University Press: Oxford, 1987.

U/W_c to 2.5,[38] placing the transition beyond the experimentally observed range for K_3C_{60}.

As W depends on inter-fulleride separation whereas U is an intramolecular quantity, the ratio U/W can be considered to increase with lattice parameter within the isostructural A_3C_{60} series. The electronic properties of the expanded fcc A_3C_{60} fullerides reported here are thus of general importance for highly correlated systems, as the role of interelectron repulsion is further enhanced over K_3C_{60}. The Knight shift of 46 ppm for $Cs_{2.68}Rb_{0.32}C_{60}$ yields a value of $N(E_f)$ of 12.42 states eV^{-1} C_{60}^{-1} $spin^{-1}$, larger than 9.09 states eV^{-1} C_{60}^{-1} $spin^{-1}$ derived from the Knight shift of K_3C_{60}, as expected due to reduction of W by the enhanced inter-fulleride separation.

Both K_{iso} and χ_{Pauli} determined from magnetization and EPR measurements are proportional to the density of states at the Fermi energy enhanced by interelectron repulsion, N_χ, over the bare value N_b in the absence of these correlations. This can be quantitatively expressed as

$$1/N_b = 1/N_\chi + I \quad (1)$$

where I is the Stoner parameter, recently determined to be 0.03 (spin eV C_{60}) for fullerides with lattice parameters between Na_2CsC_{60} and Rb_3C_{60}.[39] The experimentally determined density of states scaling

$$N_b(E_f) = \frac{\alpha}{d}\exp\left(\frac{d}{\beta}\right) \quad (2)$$

$\alpha = 3.2 \times 10^{-4}$ states eV^{-1} C_{60}^{-1} $Å^{-1}$, $\beta = 0.25$ Å, and $d = (a/2^{1/2}) - 6.95$ is the inter-fulleride distance)[39] predicts that $N_b(E_f)$ should increase to 37.5 states eV^{-1} C_{60}^{-1} $spin^{-1}$ in $Cs_{2.68}Rb_{0.32}C_{60}$. This value is sufficiently close to the inverse of the Stoner parameter itself to make N_χ derived from this predicted N_b by eq 1 divergent and unphysical. The density of states dependence on separation (2) derived for the smaller A_3C_{60} phases cannot describe the expanded A_3C_{60} metals reported here. The gentler $N \alpha \exp((d/0.58))$ dependence of Satpathy et al.[40] predicts $N_b = 1.6$ N_b (K_3C_{60}). The upper limit on N_b of $Cs_{2.68}Rb_{0.32}C_{60}$ is N_χ itself, 12.4 states eV^{-1} C_{60}^{-1} $spin^{-1}$, which would give a scaling exponent β of 0.61 Å in (2) from the bandwidth reduction to 73% of the K_3C_{60} value. The most physically acceptable approach is to adopt the Stoner parameter $I = 0.03$ to estimate $N_b = 9.1$ states eV^{-1} C_{60}^{-1} $spin^{-1}$, a 14% enhancement over K_3C_{60}. The N_b values derived from published Knight shift data[11] and the present expanded phases give $\beta = 1.08$ Å. This discussion assumes that the chemical shift of a C_{60}^{3-} anion is independent of inter-fulleride distance: in view of the nonlinear variation of the effectiveness of screening within the t_{1u} band on distance, this may not be appropriate.

This band narrowing is consistent with the increase in inter-fulleride separation over previously known A_3C_{60} systems but does not produce a direct transition from a normal metal/BCS superconductor to a Mott−Hubbard insulator. As fulleride metals are highly correlated, and the less expanded $(NH_3)K_{3-x}Rb_xC_{60}$ phases are insulators at low temperature,[41] this point is important. The absence of a transition to a Mott−Hubbard insulating ground state in the expanded cubic A_3C_{60} phases, together with recent results on antiferromagnetic ordering in the $(NH_3)(K_{3-x}Rb_x)C_{60}$ phases,[41] demonstrates that both site symmetry and electronic bandwidth are important in determining the ground state of a highly correlated low electron density metal. The tetragonal $(NH_3)K_3C_{60}$ phase[42] has a volume per fulleride anion of 760 $Å^3$ and is metallic between 300 and 40 K with a 43 ppm Knight shift. It both orders antiferromagnetically[43] and undergoes a metal−insulator transition at 40 K.[44,45] This is ascribed to the onset of a spin density wave opening a gap at the Fermi level. The Knight shift is comparable with that of cubic Rb_3C_{60}, which is stable with respect to the metal−insulator transition and has a very similar fulleride density. $(NH_3)Rb_3C_{60}$ is an insulator at all temperatures[41] with a volume per C_{60}^{3-} anion of 789 $Å^3$, showing that orthorhombic symmetry at the same conduction electron density as superconducting cubic $Cs_{2.65}Rb_{0.35}C_{60}$ is sufficient to completely localize the t_{1u} electrons. The band narrowing on expansion of A_3C_{60} to form $(NH_3)A_3C_{60}$ is therefore not solely responsible for the suppression of superconductivity, as the expanded fcc phases reported here have lower fulleride density yet retain metallic and superconducting character. In a cubic fulleride at 790 $Å^3$ per C_{60}^{3-}, the t_{1u} bandwidth is greater than the critical value of U/2.5 (~0.25 eV) in the orbitally degenerate Hubbard model. Lowering the point symmetry of the C_{60}^{3-} anion to *mmm* in the $(NH_3)A_3C_{60}$ phases completely lifts the t_{1u} orbital degeneracy, so the relevant bandwidth W_c is now that of the nondegenerate Hubbard model ($W_c \sim U \sim 1$ eV). The t_{1u} bandwidth is less than the on-site repulsion in all A_3C_{60} systems, so once the key t_{1u} degeneracy stabilizing the metallic state is lost, the t_{1u} electrons become localized in the orthorhombic ammoniated phases. The existence of metallic cubic and insulating orthorhombic fullerides with the same t_{1u} electron carrier density shows the importance of orbital degeneracy in the competition between itinerant and localized electron behavior in narrow band systems.

The expanded A_3C_{60} compounds remain metallic and superconducting but increasing the inter-fulleride separation, and thus the measured density of states at the Fermi level, decreases T_c. This contrasts with the behavior at smaller lattice parameters and contradicts the predictions of the weak-coupling BCS−McMillan theory widely used to interpret fulleride superconductivity.[36] There are three conventional explanations for this behavior. The measured reduction of T_c due to Josephson links has been dealt with in the results section: identification of the higher T_c with the intragrain transition temperature accounts for this possibility. T_c decreases rapidly as the fulleride anion charge[46,47] is raised or lowered from the "ideal" value of 3, but the Raman measurements show that all the superconducting phases here have an anion charge of 3^-. The analytical data do not entirely rule out NH_3 concentrations of less than 4% per formula unit, which have been suggested to suppress T_c in Rb_3C_{60}.[17] The Rietveld analysis and observation of inter- and intragrain T_c's both support the attribution of the observed T_c's to ammonia-free $Cs_{3-x}A_xC_{60}$ compositions. It is important to bear in mind in the following discussion that the presence of

(38) Gunnarsson, O.; Koch, E.; Martin, R. M. *Phys. Rev. B* **1996**, *54*, R11026.
(39) Robert, J.; Petit, P.; Yildirim, T.; Fischer, J. E. *Phys. Rev. B* **1998**, *57*, 1226−1231.
(40) Satpathy, S.; Antropov, V. P.; Andersen, O. K.; Jepsen, O.; Gunnarsson, O.; Lichtenstein, A. I. *Phys. Rev. B* **1992**, *46*, 1773−1793.
(41) Takenobu, T.; Muro, T.; Iwasa, Y.; Mitani, T. *Phys. Rev. Lett.* **2000**, *85*, 381.
(42) Rosseinsky, M. J.; Murphy, D. W.; Fleming, R. M.; Zhou, O. *Nature* **1993**, *364*, 425−427.
(43) Prassides, K.; Margadonna, S.; Arcon, D.; Lappas, A.; Shimoda, H.; Iwasa, Y. *J. Am. Chem. Soc.* **1999**, *121*, 11227−11228.
(44) Allen, K. M.; Heyes, S. J.; Rosseinsky, M. J. *J. Mater. Chem.* **1996**, *6*, 1445−1447.
(45) Iwasa, Y.; Shimoda, H.; Palstra, T. T. M.; Maniwa, Y.; Zhou, O.; Mitani, T. *Phys. Rev. B* **1996**, *53*, 8836−8839.
(46) Yildirim, T.; Barbedette, L.; Fischer, J. E.; Lin, C. L.; Robert, J.; Petit, P.; Palstra, T. T. M. *Phys. Rev. Lett.* **1996**, *77*, 167−170.
(47) Kosaka, M.; Tanigaki, K.; Prassides, K.; Margadonna, S.; Lappas, A.; Brown, C. M.; Fitch, A. N. *Phys. Rev. B* **1999**, *59*, R6628−R6630.

small concentrations of second phases can produce suppression of T_c by proximity effects and that only suggestive rather than conclusive evidence that this is not occurring is available.

Assuming an intrinsic origin for the observed T_c values, the dependence of the superconducting transition temperature on the density of states at the Fermi level changes sign as the inter-fulleride separation increases, as shown in Figure 8b. The $a = 14.57$ Å phase $Cs_{2.26}K_{0.74}C_{60}$ has a higher T_c than Rb_3C_{60} expected from its larger Knight shift, but both $Cs_{2.68}Rb_{0.32}C_{60}$ and $Cs_{2.38}K_{0.62}C_{60}$ have lower T_c despite the higher $N(E_f)$. The observation that the first new point here follows the extrapolated trend from the smaller *a* phases indicates a crossover in the electronic structure to a family of large *a* superconductors in which the distance dependence of T_c is inverted. In any mean-field pairing theory, the density of states dependence will change sign when W becomes less than the pairing energy E_{pair} (estimated at 0.1 eV in electron−phonon coupling theories[36]), representing a crossover to the "preformed pair" strong coupling theories. The measured Knight shifts suggest that the t_{1u} bandwidths in these expanded phases are not small enough for this to occur, as this would require a reduction in the t_{1u} bandwidth to 20% of its value in K_3C_{60}.

The proximity to the $(NH_3)A_3C_{60}$ localized electron insulators suggests that the explanation for the inverted dependence of T_c upon $N(E_f)$ lies in the interelectron repulsion. Interelectron repulsion is introduced into quantitative treatments of T_c via the parameter μ^*, which is assumed to be constant across the A_3C_{60} series. Recent theoretical work[48] indicates that, for metallic and superconducting fullerides close to the Mott−Hubbard transition, the reduction of the μ^* parameter in the McMillan equation[49] (3) by charge screening within the t_{1u} band is critical to the interpretation of the observed behavior.

$$T_c = \frac{\omega_{ph}}{1.2} \exp\left[\frac{-1.04(1+\lambda)}{\lambda - \mu^*(1+0.62\lambda)}\right] \qquad (3)$$

Here $\lambda = N(E_f)V$, where V is the electron−phonon coupling energy and ω_{ph} is the mean frequency of the phonons producing the pairing. For U/W <2, μ^* is reduced from 9 to 0.3 by screening, whereas for 2 < U/W < 2.5, this screening becomes inefficient, resulting in μ^* increasing strongly with inter-fulleride separation. This breakdown in the distance independence of μ^* at large inter-fulleride separation is entirely consistent with the superconducting behavior observed in the expanded A_3C_{60} fullerides. Within this scenario, the 30 K T_c of Rb_3C_{60} arises from $\lambda = 1.5$, $\omega_{ph} = 600$ K, and $\mu^* = 0.3$: a 10% increase in μ^* upon expansion to $Cs_{2.68}Rb_{0.32}C_{60}$ is sufficient to outweigh the increase in λ derived from the measured $N(E_f)$ and to suppress T_c to the observed value of 27K. This qualitative calculation indicates that the increase of μ^* as U/W approaches the value required for electron localization is able to explain the observed maximum in T_c in the fcc A_3C_{60} phases. The increased interelectron correlation upon expansion does not produce a Hubbard insulator due to the t_{1u} degeneracy, but is manifested as a qualitative change in the dependence of T_c upon the density of states at the Fermi level.

The intrinsic interpretation of the observed T_c values indicates the existence of two fcc A_3C_{60} families with different $N(E_f)$ dependencies of T_c. This points to a rather complex electronic structure in the fullerides near their highest superconducting transition temperatures, as even within the fcc A_3C_{60} series there appears to be no simple dependence of T_c on inter-fulleride separation. The present observations strengthen the case for comparison with the cuprates, where the dependence of T_c on the copper oxidation state changes sign with increasing oxidation state. Cs_3C_{60} under pressure with a bcc structure has a smaller volume per fulleride anion[4] than $Cs_{2.68}Rb_{0.32}C_{60}$ yet has a higher superconducting transition temperature of 40 K. The superconducting transition temperatures of C_{60}^{3-} phases therefore clearly depend on the mode of inter-fulleride overlap as well as the density, as has previously been found for the lower T_c $Na_2Cs_{1-x}Rb_xC_{60}$ phases.[50] There is no universal dependence of T_c on density even within the $Fm\bar{3}m$ symmetry family where the setting angle of the fulleride anions remains independent of lattice parameter. The breakdown of the universal relationship can be attributed to the increased importance of interelectron repulsion as the Mott−Hubbard transition is approached upon expansion. The unique aspect of the fullerides is that the t_{1u} orbital degeneracy allows metallic states to survive at U/W values that would otherwise produce localization, allowing the influence of strong correlation on superconductivity to be investigated.

The pronounced dependence of T_c on detailed structure rather than simple density should motivate the search for new structural families containing C_{60}^{3-} anions in electronic contact. The maximum in T_c as a function of fulleride density and the proximity between the highest transition temperature and the metal−insulator transition in $(NH_3)K_3C_{60}$ driven by electron repulsion in the fullerides may strengthen comparisons with the cuprates, where antiferromagnetic Cu^{II} Mott insulators are the parent phases and T_c peaks at optimal oxidation states and Cu−O distances that differ significantly within each family of materials.[51]

Acknowledgment. We thank the Leverhulme Trust and the U.K. EPSRC GR/M04006 for supporting this work. Dr S.J. Heyes is thanked for his assistance with the MAS NMR measurements.

Supporting Information Available: Plot of the Rietveld refinement of $Cs_{2.66}Rb_{0.34}C_{60}$ from synchrotron X-ray data and the resulting refined parameters; detailed description of the magnetization and critical field data for $Cs_{2.68}Rb_{0.32}C_{60}$, plus graphics of the data (PDF). This material is available free of charge via the Internet at http://pubs.acs.org.

JA002861D

(48) Koch, E.; Gunnarsson, O.; Martin, R. M. *Phys. Rev. Lett.* **1999**, *83*, 620−623.
(49) McMillan, W. L. *Phys. Rev.* **1968**, *167*, 331.
(50) Yildirim, T.; Fischer, J. E.; Dinnebier, R.; Stephens, P. W.; Lin, C. L. *Solid State Commun.* **1995**, *93*, 269−274.
(51) Cava, R. J. *J. Am. Ceram. Soc.* **2000**, *83*, 5−28.